Received: 29 November 2022 | Revised: 27 February 2023 | Accepted: 24 March 2023

DOI: 10.1002/jnr.25197

RESEARCH ARTICLE

JOURNAL OF Neuroscience Research

Zebrafish *dnm1a* gene plays a role in the formation of axons and synapses in the nervous tissue

Cinzia Bragato[1] | Anna Pistocchi[2] | Gianfranco Bellipanni[3,4] | Stefano Confalonieri[5] | Jorune Balciuniene[4] | Federica Maria Monastra[2] | Silvia Carra[6] | Giovanni Vitale[2,7] | Paride Mantecca[1] | Franco Cotelli[8] | Germano Gaudenzi[7]

[1]Department of Earth and Environmental Sciences, POLARIS Research Center, University of Milano-Bicocca, Milan, Italy

[2]Dipartimento di Biotecnologie Mediche e Medicina Traslazionale, Università degli Studi di Milano, Milan, Italy

[3]Sbarro Institute for Cancer Research and Molecular Medicine, College of Science and Technology, Temple University, Philadelphia, Pennsylvania, USA

[4]Department of Biology, Center for Biotechnology, College of Science and Technology, Temple University, Philadelphia, Pennsylvania, USA

[5]IEO, European Institute of Oncology IRCCS, Milan, Italy

[6]Laboratory of Endocrine and Metabolic Research, IRCCS, Istituto Auxologico Italiano, Milan, Italy

[7]Laboratory of Geriatric and Oncologic Neuroendocrinology Research, IRCCS, Istituto Auxologico Italiano, Milan, Italy

[8]Department of Biosciences, University of Milan, Milan, Italy

Correspondence
Cinzia Bragato, Department of Earth and Environmental Sciences, POLARIS Research Center, University of Milano-Bicocca, Piazza della Scienza 1, 20126, Milan, Italy.
Email: cinzia.bragato@unimib.it

Germano Gaudenzi, Laboratory of Geriatric and Oncologic Neuroendocrinology Research, IRCCS, Istituto Auxologico Italiano, Milan 20100, Italy.
Email: g.gaudenzi@auxologico.it

Abstract

Classical dynamins (DNMs) are GTPase proteins engaged in endocytosis, a fundamental process for cargo internalization from the plasma membrane. In mammals, three *DNM* genes are present with different expression patterns. *DNM1* is expressed at high levels in neurons, where it takes place in the recycling of synaptic vesicles; *DNM2* is ubiquitously expressed, while *DNM3* is found in the brain and in the testis. Due to the conservation of genes in comparison to mammals, we took advantage of a zebrafish model for functional characterization of *dnm1a*, ortholog of mammalian *DNM1*. Our data strongly demonstrated that *dnm1a* has a nervous tissue-specific expression pattern and plays a role in the formation of both axon and synapse. This is the first in vivo study that collects evidence about the effects of *dnm1a* loss of function in zebrafish, thus providing a new excellent model to be used in different scientific fields.

KEYWORDS

classical dynamins, dnm1a, vesicular transport protein, zebrafish embryos, nervous tissue, neurodevelopment, zebrafish AB strain (RRID:ZIRC_ZL1), Fiji software (RRID:SCR_002285), mouse anti-acetylated tubulin (RRID:AB_609894), developmental and epileptic encephalopathy (DEE) disease, DAB (RRID:AB_2335241), pBluescript SK- (RRID:Addgene_12306), Prism GraphPad Software (RRID:SCR_002798)

[Correction added on June 21, 2023 after first online publication. The fifth author's last name has been corrected from "Jorune Balciunie" to "Jorune Balciuniene."]

Franco Cotelli and Germano Gaudenzi are co-last authors.

Edited by Junie Paula Warrington and Sokol Todi. Reviewed by Vasileios Toulis.

1 | INTRODUCTION

Clathrin-mediated endocytosis (CME) is the most important endocytic way for the internalization of cargoes from the plasma membrane of eukaryotic cells into the cytoplasm (Kaksonen & Roux, 2018), and plays an important role in nerve terminals, where is involved in the recycling of synaptic vesicles after the release of neurotransmitters (Cousin, 2017). Several proteins are engaged in this process, such as the classical dynamins (DNMs) (Ferguson & De Camilli, 2012). These large GTPases are characterized by five typical domains, as a highly conserved amino-terminal GTPase domain, that binds and hydrolyses GTP, a middle domain with potential self-assembly properties, a pleckstrin homology (PH) domain involved in membrane binding, a GTPase effector domain (GED) that stimulates the GTPase activity and participates in self-assembly, and a carbossi-terminal proline/arginine-rich domain (PRD) that recruits other proteins through their SH3 domains (Ramachandran & Schmid, 2018; Zhang et al., 2020). It is currently known that DNMs assemble into helical polymers at the necks of clathrin-coated endocytic pits and mediate fission of the underlying tubular membrane to generate a free endocytic vesicle (Ferguson & De Camilli, 2012).

Originally, DNMs have been linked to endocytosis following studies on the temperature-sensitive *Drosophila* mutants' *shibire*, in which a mutation in the *dynamin* mammalian homolog is causing a block of CME. In a restrictive temperature condition, the nerve terminals of *shibire* mutants display the lack of synaptic vesicles and the accumulation of pits not coated with clathrin. Moreover, an electron-dense collar of oligomerized dynamin is visible around the narrow necks (Chen et al., 1992; Hinshaw & Schmid, 1995). Interestingly, *shibire* mutations are causing a pleiotropic defect of endocytosis in a number of other cell types (Koenig & Ikeda, 1989). Like *shibire* mutants, mammalian cells overexpressing dominant-negative mutant forms of dynamin (e.g., dynamin K44) shows an impairment of coated vesicle budding (Damke et al., 1994).

Although a single *dynamin* gene has been identified in *Drosophila* and *Caenorhabditis elegans* (Chen et al., 1991; Clark et al., 1997; van der Bliek & Meyerowitz, 1991), three *DNM* genes with specific expression patterns are present in mammals. *DNM1* is expressed at high levels in neurons. *DNM2* is ubiquitously expressed, while *DNM3* is found in the brain, but at lower levels than *DNM1*, and in the testis (Ferguson & De Camilli, 2012).

In the teleost zebrafish (*Danio rerio*) two co-orthologs of human *DNM2*, named *dnm2a* and *dnm2b*, are present and involved in the development of different systems (Bragato et al., 2016; Gibbs et al., 2013). At present, no functional studies have been conducted in this model system concerning the functional role of *dnm1*. In this work, we addressed the functional characterization of the zebrafish *dnm1a* gene, ortholog of the mammalian *DNM1*. Indeed, zebrafish is an ideal vertebrate model to provide insights into the in vivo developmental roles of genes. This is due to the ease of manipulation for developmental studies, its genetic simplicity, and the conservation of genes in comparison to mammals (Kimmel et al., 1995; Shehwana & Konu, 2019).

Significance

Zebrafish is a powerful experimental model used worldwide in many research fields. It is very suitable in investigating genes implications, which are sometimes still unknown. In this paper, we reported for the first time evidences about *dnm1a* involvement in zebrafish neurodevelopment. Being *dnm1a* an ortholog of mammalian *DNM1*, its functional characterization can pave the way to the use of zebrafish as animal model for studying pathologic mechanisms related to *DNM1* gene defects, as developmental epileptic encephalopathy (DEE), and consequently for efficiently unveiling new therapeutic targets.

In particular, we focused on the role of *dnm1a* in embryonic development through the morpholino (MO)-based gene knockdown technology. Our data demonstrate that *dnm1a* has a nervous tissue-specific expression pattern and plays a role in the formation of both axon and neuromuscular junctions.

2 | MATERIALS AND METHODS

2.1 | Animal care

Zebrafish embryos were raised and maintained according to international (European Union Directive 2010/63/EU) and national (Italian decree n. 26 of March 4, 2014) guidelines on the protection of animals used for scientific purposes. Embryos from AB strain (RRID:ZIRC_ZL1) were injected according to the principles of Good Animal Practice as defined by Italian animal welfare regulations. All experiments were performed on embryos within 5 days postfertilization (dpf), thus not subject to animal experimentation rules according to European and Italian directives.

According to Westerfield and colleagues (1993), embryos were collected by natural spawning, staged and raised at 28°C in fish water (Instant Ocean, 0.1% methylene blue in petri dishes) containing 0.003% 1-phenyl-2-thiourea (PTU, Sigma-Aldrich, Saint Louis, MO).

The transgenic *Tg(UAS:dnm1a)* zebrafish line was generated at the Temple University, following the IACUC approval. Animals were injected according to good animal practice principles as defined by the US animal welfare regulations.

2.2 | *dnm1* identification

Ensembl genome (http://www.ensembl.org/Danio_Rerio, release 107 Jul 2022) and EST public databases (http://www.ncbi.nlm.nih.gov/BLAST) were initially queried using human DNM1 protein (NM_004408) sequence.

Two orthologs of mammalian *DNM1* were identified, named *dnm1a* and *dnm1b*, respectively.

In order to validate the transcript sequences, different approaches were used, as in silico, 5′ RACE (Rapid Amplification of cDNA ends, Invitrogen corporation, Waltham, Massachusetts, USA) and RT-PCR. Successively, the amplification products were validated by cDNA sequencing.

2.3 | Temporal expression analysis by RT-PCR

RT-PCR was performed on total RNA extracted from different developmental stages (30 embryos per sample) and adult organs using the TOTALLY RNA isolation kit (Ambion, Invitrogen corporation, Waltham, Massachusetts, USA), treated with RQ1 RNase-Free DNase (Promega, Madison, Wisconsin, USA) and oligo(dT)-reverse transcribed using Superscript II RT (Invitrogen corporation, Waltham, Massachusetts, USA), according to the manufacturer's instructions. The following primers were used for PCR reactions: *dnm1a*_fw 5′-CGAGGAGGACTTCATCGGATTTG-3′; *dnm1a*_rw 5′-CAGCTGAGGGTCCATGGAGTGC-3′; *β-actin*_fw 5′-TGTTTTCCCCTCCATTGTTGG-3′; *β-actin*_rw 5′-TTCTCCTTGATGTCACGGAC-3′.

The primers used for the *dnm1b* identification were *dnm1b_fw* 5′-AGCCTCTCCAGACCCCTTC-3′; *dnm1b_rw* 5′-CACTAATGTTCATTCTTGGCGTA-3′.

2.4 | Whole-mount in situ hybridization (WISH) and histological sections

An 1188 bp long EST (GenBank accession numbers: BI706758) was identified and then cloned into pBluescript SK- (RRID:Addgene_12306). The EST sequence specifically matched a portion of *dnm1a* transcript, corresponding to the less similar region between classical *DNMs*. This clone was obtained from the Consortium IMAGE (4790989). The enzymes used to isolate the insert were *EcoRI* and *HindIII*. After enzymatic digestion, sticky-ends were refilled with Klenow (New England Biolabs, Ipswich, Massachusetts, USA) and subsequently the open plasmid was ligated with "Quick Ligase kit" (New England BioLabs, Ipswich, Massachusetts, USA) following manufacturer's instructions. The pBluescript SK- carrying *dnm1a* sequence was linearized with *BamHI*, the antisense RNA was synthesized using T7 RNA polymerase and labeled with digoxigenin-UTP (Roche, Basel, Switzerland). For the synthesis of the sense probe, the enzyme *XhoI* was used and the plasmid transcribed by the T3 polymerase (Roche, Basel, Switzerland). Whole-mount in situ hybridization was carried out as described (Köster & Fraser, 2001) on embryos fixed for 2 h in 4% paraformaldehyde/phosphate-buffered saline, then rinsed with PBS-Tween, dehydrated in 100% methanol and stored at −20°C until processed.

For histological sections, stained embryos were refixed in 4% PFA, dehydrated and stored in methanol, wax embedded and sectioned (8 μm).

WISH for *dnm1b* was carried out using a specific 244 bp riboprobe made by in vitro transcription with T7 or SP6 RNA polymerase (Promega, Madison, Wisconsin, USA). Template was generated by PCR using the following primers: *dnm1b_fw* 5′-GGCTGGTTTACATTGGCAGT-3′ and *dnm1b_rw* 5′-CTGTGTGTGCTTGTGTGTCA-3′. *Dnm1b* amplicon was then cloned into pGEM-T-Easy Vector plasmid (Promega, Madison, Wisconsin, USA) and cutted with the enzymes *ApaI* and *BstXI* (New England BioLabs, NEB). WISH was carried out as previously described (Thisse & Thisse, 2014), following a specific protocol for short riboprobes (Narayanan & Oates, 2019).

2.5 | Immunohistochemistry and AChR labeling

For immunohistochemistry on fixed embryos, the following primary antibodies were used: mouse anti-DNM1 (E-11, Santa-Cruz Biotechnology, Dallas, Texas, USA), mouse anti-Acetylated tubulin (RRID:AB_609894, Sigma-Aldrich, Saint Louis, MO, USA), and mouse anti-SV2 (Developmental Studies Hybridoma Bank, University of Iowa, Dept. of Biology, 028 BBE, 210 E Iowa Ave, Iowa City, IA 52242-1324). The second day, embryos were treated with biotinylated or fluorescent secondary antibodies (Vector Laboratories, Newark, California, USA). Postsynaptic regions were labeled with Alexa Fluor 594 conjugated α-bungarotoxin (Invitrogen corporation, Waltham, Massachusetts, USA) for 30 min as described in Bragato et al. (2021).

2.6 | Quantification of DNM1 signal

To quantify the anti-DNM1 level revealed by DAB (RRID:AB_2335241), the signal area (expressed as percentages) was calculated on each image by means of Fiji (RRID:SCR_002285) software version 2.0 (http://rsb.info.nih.gov/nih-image/) (Schindelin et al., 2012). The protocol from LSU Health Sciences Center-Shreveport Research Core Facility Chaowei Shang, Oct 2018, was applied for the quantitation. Briefly, fields occupied by the anterior part of the animal were photographed and digitized. Using the software, the Color Deconvolution and the selection of the staining of our image was used. Successively, a threshold was applied to the photographs to obtain red and black images with areas positive for DAB in red and negative areas in black. The area positive for DAB was calculated as a percentage of the entire image on each micrograph, and the mean percentage calculated. The same procedure was repeated for each group of animals, and the mean percentage calculated.

2.7 | Knockdown experiments

To perform *dnm1a* knockdown the following morpholino oligos (Gene Tools, LLC, USA) were microinjected: *dnm1a*-ATG-MO (5′-CGCCGGAGAAACTGCGCTTTATTGC-3′); *dnm1a*- I5E6-MO (5′-GTAGCCTAACGTCAGAAACACATAA-3′).

The p53-MO (5′-GCGCCATTGCTTTGCAAGAATTG-3′) was co-injected to evaluate the *dnm1a*-MOs specificity and to reduce the off-target effects (Robu et al., 2007).

Morpholinos were diluted in Danieau solution and injected at the one- to two-cell stage; the rhodamine dextran was used as vital tracer dye.

The morpholinos efficiency was assessed by Western blot and RT-PCR techniques. The primers used for RT-PCR are the following: *dnm1a*-MO-Fw 5′-CAAGAAGGACATCACTGCGG-3′ and *dnm1a*-MO-Rw 5′-TTCTTTGTGCACTGCCTGAC-3′ (805 bp).

2.8 | Western blot

Dechorionated embryos were solubilized in RIPA buffer (Radio-Immunoprecipitation Assay buffer) plus protease inhibitor and phenylmethylsulfonyl fluoride100X (PMSF). Samples were boiled for 10 min at 95° or sonicated. Twenty micrograms of protein samples were electrophoresed on 10% SDS-PAGE and transferred to nitrocellulose membranes (Bio-Rad Laboratories, Hercules, CA, USA) following the standard procedures. The membranes were blocked with 5% nonfat dry milk in TBS, pH 7.5, containing 0.1% Tween 20 (TBST) for 1 h at room temperature and subsequently incubated with the primary antibodies anti-DNM1 and anti-acetylated β-tubulin (polyclonal, Sigma-Aldrich, Saint Louis, MO, USA) used as internal control, followed by biotinylated goat anti-mouse or goat anti-rabbit, ABC-Kit Complex (DAKO, Agilent Technologies, Santa Clara, CA, USA), and ECL detection (Bio-Rad Laboratories, Hercules, CA, USA).

2.9 | Screening for embryonic motility

At 5 dpf, morphants and controls were subjected to two tactile stimulus tests. Using a needle, a gentle stimulus was applied at the tail of the larvae and elicited reactions observed under a stereomicroscope. During the first behavioral test (Test 1), embryos were touched four times consecutively, and the number of evoked escape events were recorded. In the second test (Test 2), larvae were positioned into the center of a 100 mm Petri dish located on a squared paper (5 mm square side) and the swimming distance after four touches was calculated. The cut-off of both Test 1 and 2 was first identified in wild-type control larvae.

2.10 | Generation of *Tg(UAS:dnm1a)* transgenic zebrafish

Full-length *dnm1a* cDNA was cloned from 5 dpf embryo cDNA pool as a composite of two PCR fragments. The PCR fragments were obtained using primers that were designed based on dynamin mRNA sequence as predicted in Zv9 assembly of the zebrafish genome. The primer pairs were as follows: 5′-ATGGGGAACCGCGGGATGG-3′ and 5′-TTCGAGCTCCTCCAGAAAGCTC-3′; 5′-GAGCTTTCTGGAGGAGCTCGAA-3′ and 5′-TCAGGGACCACTGGGCACACT-3′.

The cDNA was cloned into a pDB790 vector (vector sequence available upon request) downstream of 14xUAS and E1b minimal promoter sequences (Balciuniene et al., 2013). The vector also contained eGFP under the control of the γ-crystalline promoter (γ-cry:eGFP) which resulted in eGFP expression in the lens and served as a marker for the transgenic construct. In addition, the whole transgenic cassette (*γcry:eGFP;UAS:dnm1a*) was flanked with Tol2 inverted repeats to facilitate transgene integration into the zebrafish genome. The *UAS:dnm1a* zebrafish line was generated using standard Tol2 transgenesis protocol (Suster et al., 2009). Briefly, one-cell stage embryos were injected with 25 pg of the recombinant plasmid and 25 pg of Tol2 RNA. At 3 dpf, injected fish were screened for eGFP expression in the lens. Positives for lens GFP fish were raised and outcrossed to establish three independent *Tg(UAS:dnm1a)* zebrafish lines.

2.11 | Rescue experiments

To achieve the *dnm1a* transgene expression in neurons, the Tg(UAS:*dnm1a*)$^{y/+}$ fish line was crossed to a driver fish line (ns-f^{tpl006Gt}), expressing GAL4 and GFP under the control of endogenous pan-neuronal nsf promoter (Woods et al., 2006). The progeny was then injected with *dnm1a*- I5E6-MO at one- to two-cell stage. At 3 days postfertilization, embryos were screened based on the GFP expression, and divided into three experimental groups. Embryos without GFP expression (Group 1) and embryos expressing GPF in the lens only (Group 2) were considered controls, while the *dnm1a*-expressing fish, characterized by GFP expression in the nervous system and lens, were included in the Group 3. At 5 dpf, two motility tests (Test 1 and Test 2) were performed on the three experimental groups as above described. The embryos observed throughout the two motility tests were $n = 90$ for each experimental group, collected during three different experiments.

2.12 | Thin, semithin, and ultrathin sections

Morphants and control embryos were dechorionated, anesthetized in Tricaine (MS-222), and fixed in 0.1 M sodium cacodylate, 2% paraformaldehyde, and 2.5% glutaraldehyde. After fixation, embryos were rinsed in 0.1 M sodium cacodylate, postfixed in 1% osmium tetroxide in 0.1 M sodium cacodylate. During dehydration specimens for transmission electron microscope (TEM) were prestained with a saturate solution of uranyl acetate, then embedded in Epon 812 Araldite and sectioned with a Reichert Ultracut E. Section for electron microscope was stained with uranyl acetate (aqueous solution) and lead citrate and examined in a Jeol 1010 SX electron microscope. Sections for light microscopy (0.5–1 μm in thickness) were stained with gentian violet.

2.13 | Statistics

Statistical analyses were performed using GraphPad Prism 9.2.0.332 (GraphPad Software, RRID:SCR_002798). The differences between groups in rescue experiments (Ctrl not injected, Group 1, Group 2, and Group 3) were assessed by Chi-square test (Table 2). Differences in axon defects, as trajectory, grade, extension, and branching, were assessed by the Chi-square test (Table 3). Differences in DNM1 signal between STD-Ctrl-MO and *dnm1a*-MOs were assessed using the two-tailed Student's *t* test (Figure 3A, panel d).

3 | RESULTS

3.1 | Identification of *dnm1a*

The transcript sequence of *dnm1a* (GenBank EF395230.1), previously annotated as *dnm1*, was identified by our group combining in silico and molecular methods. Gene structure was reconstructed by aligning transcript and genomic sequences (Figure 1). By sequencing RT-PCR products, two sites of alternative splicing were identified. The first site includes exon 10 and 11, which had the same number of base pairs and can be alternately retained without changing the reading frame. Interestingly, the alternative splicing of these exons has also been described in mammals. The second site corresponds to exon 23 (36 base pairs), which, if retained, introduced an alternate stop codon. The deduced amino acid sequences of *dnm1a* splicing variants, analyzed by means of the CDD (conserved domain database) tool (available at https://www.ncbi.nlm.nih.gov/cdd), showed the same functional domains.

After the release of the zebrafish reference genome sequence in 2013 (Howe et al., 2013), a further zebrafish *dnm1* gene, annotated as *dnm1b* (ENSDARG00000009281; ZFIN:ZDB-GENE-100920-3), was reported as new putative ortholog of human *DNM1*. The presence of two *dnm1* paralogs in other teleost fish supported their origin from the whole-genome duplication that occurred in the teleost lineage around 320 million years ago (Koonin, 2005) (Figure S1). *dnm1a* and *dnm1b* resulted located in different portions of the chromosome 5 (*dnm1a* ch5: 1,278,092–1,421,927; *dnm1b* ch5:

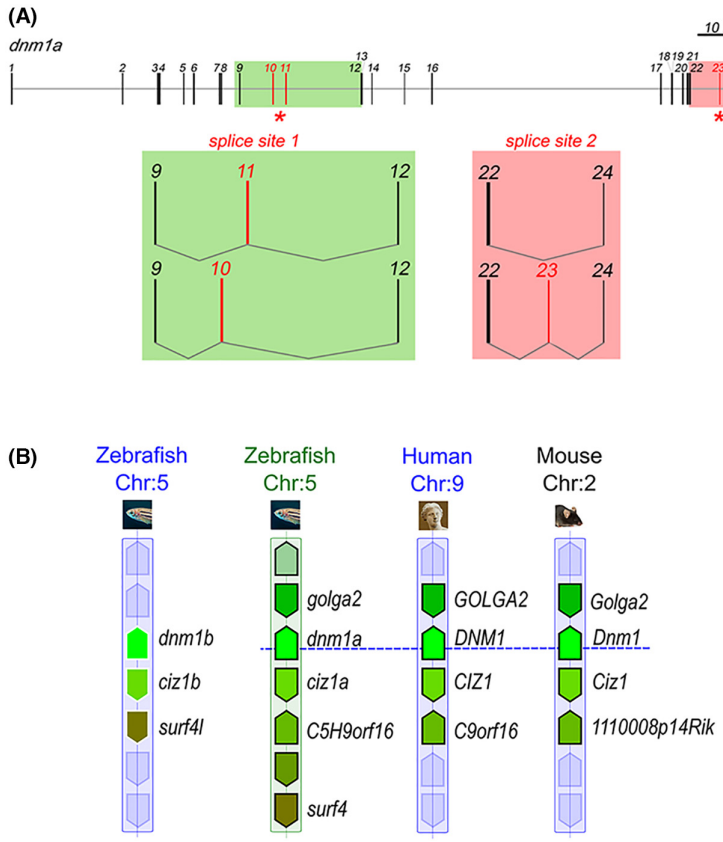

FIGURE 1 *dnm1a* synteny and alternative splicing sites. (A) Genomic organization and transcript variants of *dnm1a*. In the schematics of *dnm1a*, exons were numbered and indicated by boxes, while introns were indicated by solid lines. Red boxes indicated alternative spliced exons. Areas containing sites of alternative splicing were highlighted in green and red. Observed events of alternative splicing were represented showing retained exons at each splice site. (B) Synteny map comparing flanking regions of *dnm1* loci among zebrafish, mouse and human chromosomes (chr) was obtained through the Genomicus Phyloview browser. Genes annotated as paralogs (no surrounding line) or orthologs (with a black surrounding line) by the Ensembl database shared the same color. Syntenic genes was detected in flanking regions of both *dnm1a* and *dnm1b*, suggesting they are co-orthologs of mammalian single copies. However, genomic context of *dnm1a* is more similar to human *DMN1* and murine *Dnm1* flanking regions than *dnm1b*.

63,668,735–63,737,734). The comparison of their neighboring genomic regions to those of human and murine counterparts obtained by using the Genomicus Phyloview browser for synteny analysis (https://www.genomicus.bio.ens.psl.eu/genomicus-106.01/cgi-bin/search.pl), showed that the *dnm1a* genomic context was more similar to the human and murine *DNM1* than *dnm1b* (Figure 1B).

Unlike *dnm1a*, the presence of *dnm1b* alternative splice variants did not emerge from the sequencing of RT-PCR products.

Although both *dnm1a* and *dnm1b* displayed sequences coding for the five typical domains of classical DNMs, a multiple alignment analysis of nucleotide sequences showed that the *dnm1a* was slightly more similar to the human *DNM1* than *dnm1b* (81% vs. 78% of nucleotide identity).

3.2 | Analysis of *dnm1a* spatio-temporal expression

RT-PCR assays using total RNAs extracted from embryos at different embryonic and larval stages (ranging from the first cleavage stages to early larval period) and from different adult organs were performed. During embryo development, *dnm1a* mRNA was identified starting from the tail bud stage (10 hpf, hours postfertilization) through 5 dpf (days postfertilization) (Figure 2A,a). In the adult, zebrafish *dnm1a* transcript was detected in the brain, eyes, and liver (Figure 2A,b).

To describe the *dnm1a* spatial expression pattern during zebrafish embryonic development, WISH assays were performed on embryos at developmental stages ranging from 10 hpf to 5 dpf. The antisense riboprobe has been synthesized to target a region of *dnm1a* transcript sharing low nucleotide identity with *dnm1b*, comprising a portion of the 3′UTR and the sequence coding for the C-terminal domains. Not significant hybridization signals were detected before 20-somite stage (19 hpf). At 24 hpf *dnm1a* transcript was localized in the epiphysis and in three large bilateral clusters in anterior telencephalon (dorso rostral cluster) and on the floor of the diencephalon (ventro rostral cluster) and mesencephalon (ventro caudal cluster). Expression was also detected in the hindbrain and in the spinal cord, and in six bilateral spots, corresponding to the anterior and posterior lateral line and trigeminal ganglia (Figure 2C). Transverse histological sections of 24 hpf embryos trunk, showed *dnm1a* expression in the medio-ventral portion of the spinal cord, corresponding to the area of developing motor neuron nuclei. Starting from 2 dpf, the *dnm1a* expression pattern in the CNS became progressively more complex compared to the 24 hpf being more widely distributed in the CNS with spatially restricted areas. A hybridization signal was detected in the spinal cord and in the pallium area as shown by transverse histological sections at the level of the telencephalon of embryos from 2 to 5 dpf. The *dnm1a* transcript was present in the preoptic area, which represents an intermediate region between telencephalon and diencephalon, and in the hypothalamus, as well as in two areas corresponding to the ventral part of the posterior tuberculum and to the dorsal thalamus. A number of *dnm1a* expressing cells were detected in the mesencephalon tegmentum and in the optic tectum, while in the hindbrain the signal was less distributed and more diffused (Figure 2C).

Moreover, *dnm1a* expression was detected also in the neural part of the eye. Histological sections of 2 dpf embryos showed a signal in the retina, in particular in the inner and outer plexiform layers and in the ganglion cells layer.

The localization of Dnm1a protein during embryonic development was further investigated taking advantage of a monoclonal antibody against human *DNM1* that recognizes a region present in the zebrafish Dnm1a (Figure 2D). Immunopositive spots corresponding to developing glomeruli in the telencephalon were observed in embryos at 3 days postfertilization (dpf). Moreover, *dnm1a* signal was found in the hindbrain and in the spinal cord in the anterior and postoptic commissure. A faint signal was detected in motor neuron axons and in cephalic ganglia. In accordance with the WISH staining, at the stage of 3 dpf Dnm1a protein was observed in the retina, both in the inner plexiform layer and outer plexiform layer.

3.3 | Analysis of *dnm1b* spatio-temporal expression

As for *dnm1a*, the *dnm1b* temporal expression was firstly analyzed by RT-PCR assays on maternal and zygotic developmental stages. *dnm1b* mRNA resulted expressed starting from 80% epiboly stage, suggesting a nonmaternal origin of the transcript (Figure S2).

WISH assays were further performed with an RNA antisense probe targeting a 244 bp long sequence within the 3′-UTR of the transcript. The probe was specifically designed to assess the spatial distribution of *dnm1b*. A clear expression in the developing nervous system did not emerged from our analyses on dnm1b. A faint and widespread signal was detected only after long-lasting WISH staining. However, the signal localization resulted completely overlapping with that of control riboprobe, thus suggesting the presence of a possible unspecific background staining.

3.4 | *dnm1a* is necessary for embryo's motility

To analyze the function of *dnm1a* during zebrafish embryonic development, a knockdown approach was used. The microinjection of two-specific *dnm1a* antisense morpholino, a *dnm1a*-ATG-MO targeting the ATG region of the transcript and a *dnm1a*-I5E6-MO, targeting the splice site between intron 5 and exon 6, was performed. From this point, the expression *dnm1a*-MO indistinctly denotes the two oligomers.

In each experiment, the *dnm1a*-MOs were coinjected with p53 morpholino, in order to reduce specifically the cell death induced by MO off-targeting (Robu et al., 2007).

Embryos at one-cell stage were microinjected with both morpholino at the concentration of .3, .5, and .75 mMol. The embryos injected with both *dnm1a*-morpholino (morphants) were compared to control embryos (STD-Ctrl), obtained by the injection of the

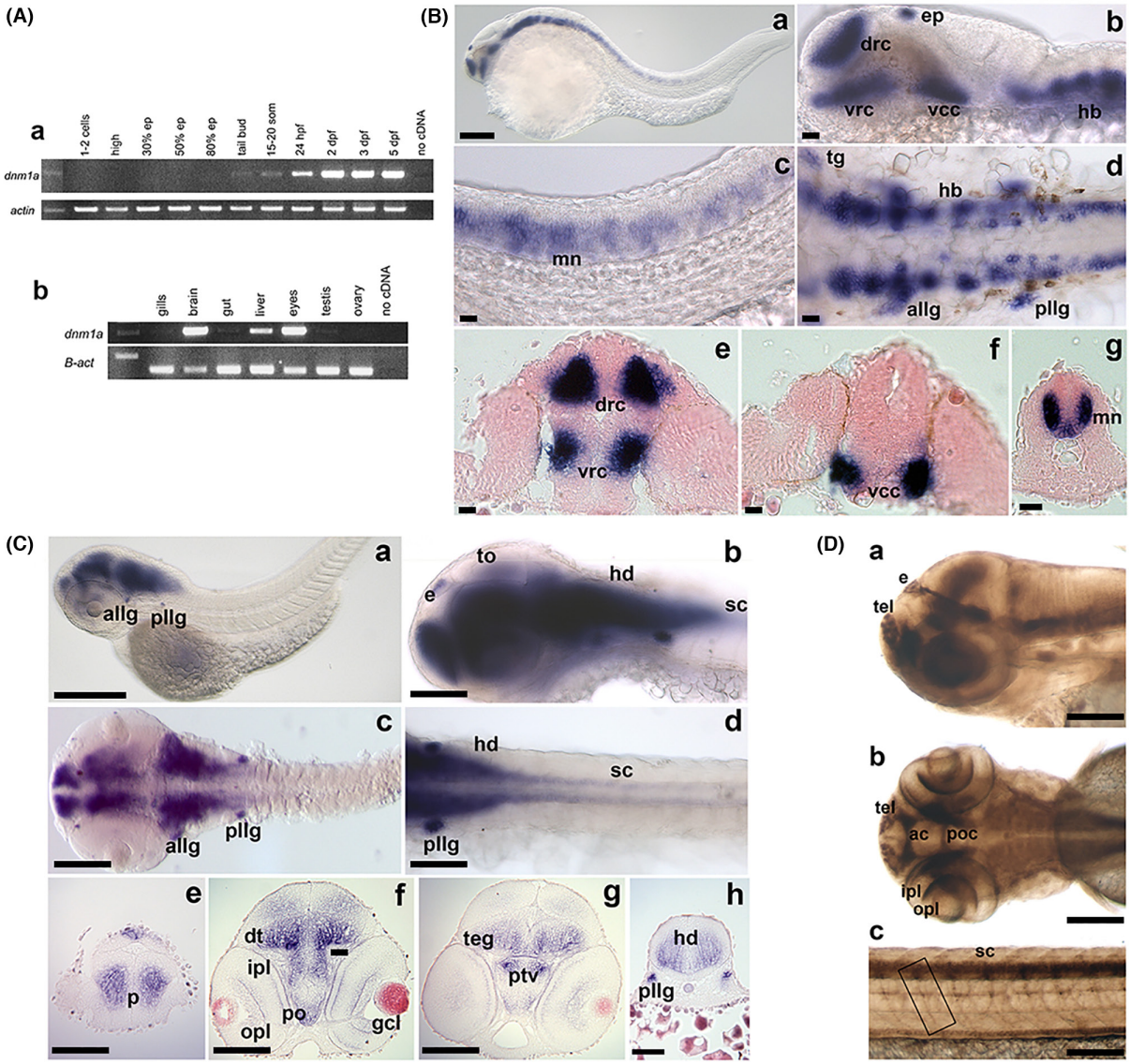

FIGURE 2 Panel A. *dnm1a spatio-temporal expression*. RT-PCR assays using total RNAs extracted from embryos at different embryonic and larval stages (ranging from the first cleavage stages to early larval period) and from different adult organs were performed. (a) During embryo development, *dnm1a* mRNA was identified starting from the tail bud stage (10 hpf, hours postfertilization) through 5 dpf. Scale bar 250 μm. (b) In the adult, zebrafish *dnm1a* transcript was detected in the brain, eyes, and liver. Scale bar 250 μm. (c–g) Scale bar 250 μm. Panels B and C. *dnm1a spatial expression pattern during zebrafish embryonic development*. (B, a, e and f) At 24 hpf *dnm1a* transcript was localized in the epiphysis and in three large bilateral clusters in anterior telencephalon (dorso rostral cluster, drc) and on the floor of the diencephalon (ventro rostral cluster, vrc) and mesencephalon (ventro caudal cluster, vcc). (B, b–d and g) Strong signals were detected in the hindbrain and in the spinal cord. (B, c and g) Transverse histological sections of 24 hpf stained embryos at trunk level revealed that *dnm1a* was expressed in the medio-ventral portion of the spinal cord, corresponding to the area of developing motor neuron nuclei (mn). (B, d) At 24 hpf *dnm1a* transcript is present in six bilateral spots, corresponding to the anterior and posterior lateral line (allg and pllg) and trigeminal ganglia (tg). During later stages, *dnm1a* expression is visible in the cephalic regions of the CNS and in the ganglia-like structures. Scale bar 100 μm. (C, b and d) Starting from 2 dpf a hybridization signal in the spinal cord was detected only after an extended staining reaction time (sc). (C, e–h) Telencephalon transverse histological sections of 2 and 5 dpf larvae showed *dnm1a* expressing cells localized in the pallium area (p). (C, f) *dnm1a* is present in the preoptic area (po), and in the hypothalamus. (C, g and f) A strong signal is present in two areas corresponding to the ventral part of the posterior tuberculum (ptv) and to the dorsal thalamus (dt). (C, g) *dnm1a* expressing cells are visible in the mesencephalon tegmentum (teg). (C, b) *dnm1a* presented a slight expression in the optic tectum (to). (C, h) *dnm1a* signal is present in the hindbrain (hd). Panel D. Dnm1a *protein localization during embryonic development*. (a and b) Immunopositive spots, corresponding to developing glomeruli, in the telencephalon (tel), were observed in embryos at the developmental stage of 3 days postfertilization. Dnm1a signal is present in the hindbrain and in the spinal cord, localized in the anterior and postoptic commissures (ac and poc). (b) At 3 dpf, an increase in Dnm1a signal was observed in the retina (IPL and OPL). (c) A faint signal was detected in motor neuron axons and in cephalic structures similar to ganglia. Scale bar 250 μm.

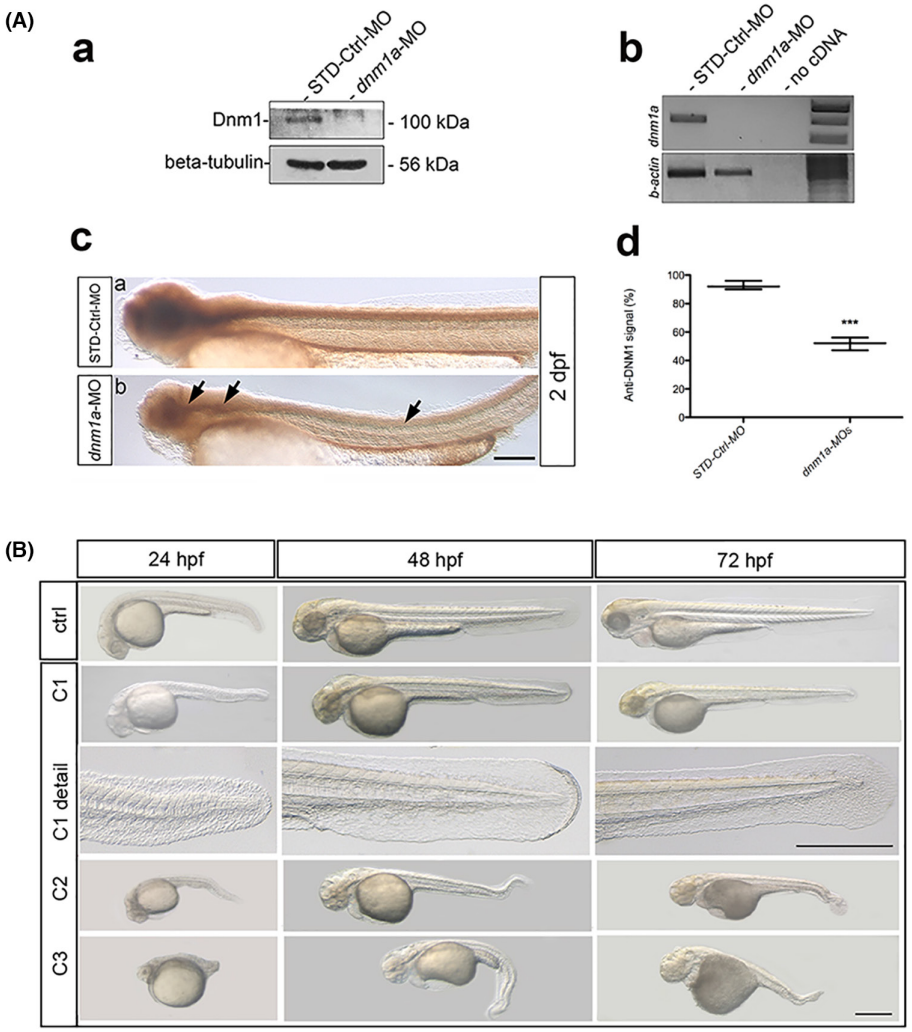

FIGURE 3 Panel A. *dnm1a* downregulation efficiency. (a) Western blot shows reduced Dnm1a (100 kDa) expression level in MO-injected embryos, with β-tubulin (56 kDa) as internal control. (b) RT-PCR agarose gel shows *dnm1a* morpholino efficiency. (c) Representative image of embryos at 2 dpf immunostained with anti-DNM1. Dnm1a signal was quantified in whole morphants and compared to control embryos at 2 dpf. Scale bar 100 μm. The Dnm1a signal was significantly reduced in morphants compared to control embryo (arrows). (d) Graph reporting the Dnm1a signal quantification from three independent experiments. The significance was calculated by two-tailed Student's *t* test,$^{***}p < .001$, $t = 13.038$, $df = 3.5165$. Panel B. *dnm1a loss of function assays*. Lateral views of uninjected and *dnm1a*-MO-injected embryos at 24 hpf, 48 hpf, and 72 hpf. Morphants displayed tail abnormalities that were subdivided into three classes: C1, C2, and C3. Magnifications of C1 class tails embryos underline the defects in somite structure. Scale bar 200 μm.

standard control morpholino, a specific oligo for *β-globin* human transcript that has not target in zebrafish.

To assess the efficacy of *dnm1a*-MOs, the Dnm1a protein level was analyzed by Western blot for the translation blocking oligomer, while the efficiency of the MO targeting the splicing site was demonstrated by RT-PCR (Figure 3A, a and b). Moreover, the *dnm1a* downregulation was demonstrated also through whole-mount immunohistochemistry assays on control and morphant embryos (Figure 3A, c). The Dnm1a signal was significantly reduced in *dnm1a*-Mos-injected embryos in comparison to STD-Ctrl-MO (*dnm1a*-ATG-MO vs. STD-Ctrl-MO, $p < .001$, $t = 13.038$, $df = 3.5165$; *dnm1a*-I5E6-MO vs. STD-Ctrl-MO, $p < .001$, $t = 12.746$, $df = 3.6697$) (Figure 3A, d).

The *dnm1a* knocked-down embryos analyzed at 24 hpf showed an altered body plan, which increased during successive developmental stages. These defects were dose dependent as the injection of increased dosages of *dnm1a*-MOs was associated with a progressive increase in tail abnormalities and mortality (Table 1). Tail defects were divided into three phenotypic classes, called C1, C2, and C3. Embryos pertaining to the C1 class showed a normal body plan, with somites characterized by slightly disrupted arrow shape. The most severe phenotypic effect was an evident curvature in tail structure. The C2 class embryos showed defects exclusively restricted to the terminal tail portion, while the C3 class phenotypes exhibit defects also in the anterior regions of the tail (Figure 3B).

The C1 class was used to perform behavioral analyses, in order to avoid motor defects being secondary to alteration of the body plan. Moreover, the touch-evoked response outcomes from morphants and controls were compared to assess the impact of *dnm1a*

TABLE 1 Concentrations of *dnm1a*-ATG-MO and *dnm1a*-I5E6-MO used.

	Concentration	Letality at 24 hpf (%)	Tail defects at 24 hpf (%)	Number of embryos
dnm1a-ATG-MO	.5 pmoli/embr	25.3	12	186
	.6 pmoli/embr	31	21	343
	.75 pmoli/embr	44.3	95	47
dnm1a-I5E6-MO	.5 pmoli/embr	24.7	14	155
	.6 pmoli/embr	37	23	286
	.75 pmoli/embr	46	87	39
STD-Ctrl-MO	.5 pmoli/embr	19.2	1	92
	.6 pmoli/embr	19	2	180
	.75 pmoli/embr	20.1	2	40
Ctrl not injected		21	1	774

Note: Increased dosages of both antisense *dnm1a*-MO were associated with a progressive increasing of mortality and tail abnormalities.

knockdown on motility. *Dnm1a*-MOs embryos showed an alteration in the evoked escape behavior, which became more severe during time. At 24 hpf *dnm1a*-MOs-injected embryos showed stiffness while starting from 48 to 72 hpf showed impaired spontaneous and touch-provoked mobility, presenting a weak escape reaction.

To validate functional results, rescue experiments were performed by knocking-down *dnm1a* in transgenic embryos expressing *dnm1a* in a large population of the spinal cord neurons. As described in Material and Methods section in detail, controls of these assays were considered embryos without transgenic expression of *dnm1a*, identifiable by the absence of fluorescence (Group 1) or expression of GFP only in the lens (Group 2). Instead, the expression of dnm1a was identified by the presence of GFP signal in both nervous system and lens (Group 3).

The effect of *dnm1a* knockdown was analyzed at 5 dpf in each group by two behavioral tests considering embryos reactivity (Test 1) and swimming distance (Test 2) after a tactile stimulation. A lower number of embryos showing normal behavioral phenotype was observed in Group 1 and 2 compared to Group 3 during three independent experiments (Table 2).

3.5 | Neuromuscular junction formation results impaired in the absence of *dnm1a* expression

Since *dnm1a*-MOs showed a motility impairment, the involvement of *dnm1a* in the neuromuscular junction (NMJ) formation was assessed. The neurite formation was analyzed in three dpf *dnm1a*-MOs, taking advantage of the acetylated tubulin antibody (Figure 4A). Different defects in the pathfinding of motor neuron axons were observed in *dnm1a*-MOs-injected embryos with a straight ventral trajectory of CaP axons (78% of injected embryos, $n=42$, $p<.01$) compared to control embryos ($n=40$). A small percentage of embryos also axons that failed to elongate (14.3% of injected embryos, $n=42$, $p<.05$, asterisk), and present an atypical curve of the terminal portion (arrowhead, Figure 4A, b). Defects observed in axon development, as trajectory grade and branch defects, besides reduced extension, are reported in Table 3.

In order to visualize NMJs, a double-stained with the presynaptic vesicles SV2, and α-bungarotoxin, which label the clusters of postsynaptic acetylcholine receptors (AChR) in the target muscle cells, was performed (Figure 4B). The colocalization of the two signals suggested that axonal projections were correctly associated with the AchR cluster in morphant and control embryos. The number of NMJs did not appear to be different in the two experimental groups. However, the distribution pattern of AChR and consequently that of NMJs appeared altered in morphants compared with controls, as a possible effect of defects in muscle organization.

3.6 | Loss of *dnm1a* affects axial muscles

Due to the motility and motor neuron axon defects observed, the axial musculature development was investigated. Before 24 hpf the distribution of *myoD* transcript in *dnm1a*-Mos-injected embryos and STD-Ctrl embryos was similar (Figure 5A).

Semithin section performed at 24 hpf showed altered slow and fast muscle fibers arrangement in *dnm1a*-MOs embryos compared to controls. (Figure 5B, b). Atrophic fibers and broad spaces were observed between muscle cells and the amount of myofibers in the muscle pioneers was reduced (Figure 5B, b, black arrow).

At 2 dpf few cells, corresponding to the adaxial cells after migration, were observed on the upper portion of the myotome (Figure 5B, d, asterisk). Moreover, slow fibers development appeared impaired (Figure 5B, d, black arrowhead). In the deep region of the myotome, large amounts of not differentiated myoblasts with a central nucleus were present (Figure 5B, d and f, white arrowhead), alongside an evident nucleolus and a few groups of disorganized myofibrils. Furthermore, in morphants were detected an altered morphology, compared to STD-Ctrl embryos.

At ultrastructural level, 72 hpf morphants showed mitochondria and nuclei in the central region of the muscle cells and regions

TABLE 2 Rescue experiments.

	Normal	Altered
Test 1 (reactivity)		
Ctrl not injected	89	1
No GFP expression (Group 1)	32***a***	58
GFP in lens only (Group 2)	32***a***	58
GFP in nervous system (Group 3)	70***a,b***	20
Test 2 (swimming distance)		
Ctrl not injected	88	2
No GFP expression (Group 1)	37***c***	53
GFP in lens only (Group 2)	32***c***	58
GFP in nervous system (Group 3)	55***c,d***	35

Note: Two behavioral tests, which considered embryo reactivity (Test 1) and swimming distance (Test 2) after a tactile stimulation. For statistical analysis, embryos from each experimental group ($n = 90$ embryos) derived from three independent experiments, were pooled. In the table are reported the number of embryos with normal behavior in not injected control embryos and after *dnm1a* knockdown. Group 1 (no GFP expression) and Group 2 (GFP expression in lens only) include morphants without expression of transgenic *dnm1a*, compared to Group 3 (GFP expression in the nervous system), in which transgenic *dnm1a* is expressed. The statistical analysis applied was the Chi-square test, with the following results. For Test 1, a significant difference was observed between "Ctrl not injected" and both "No GFP expression (Group 1)" and "GFP in lens only (Group 2)", (***a***, $p < .001$, Chi-square value = 81.92, degrees of freedom (df) = 1); the same was observed comparing "Ctrl not injected" and "GFP in nervous system (Group 3)" (***a***, $p < .001$, Chi-square value = 19.46, $df = 1$). Moreover, a significant difference was observed also between "GFP in nervous system (Group 3)" and both "No GFP expression (Group 1)" and "GFP in lens only (Group 2)" (***b***, $p < .001$, Chi-square value = 32.67, $df = 1$). Evaluating the results obtained in Test 2, a significant difference was observed between "Ctrl not injected" and "No GFP expression (Group 1)" (***c***, $p < .001$, Chi-square value = 68.10, $df = 1$) and between "Ctrl not injected" "GFP in lens only (Group 2)," (***c***, $p < .001$, Chi-square value = 78.40, $df = 1$). Moreover, a difference was observed also between "Ctrl not injected" and "GFP in nervous system (Group 3)" (***c***, $p < .001$, Chi-square value = 37.05, $df = 1$). Comparing "GFP in nervous system (Group 3)" and "No GFP expression (Group 1)" (***d***, $p = .0073$, Chi-square value = 7.20, $df = 1$) a significant difference between the two groups was observed, and even more comparing "GFP in nervous system (Group 3)" to "GFP in lens only (Group 2)" (***d***, $p < .001$, Chi-square value = 11.77, $df = 1$). In conclusion, the Group 3 showed the less severe phenotype in both tests. Thus, a partial rescue phenotype was obtained in both assays, suggesting that the paralysis phenotype is a direct cause of the knockdown of *dnm1a*.

in which myofibrils with a correct orientation were present, interrupted by extensive regions of vacuolated sarcoplasm (Figure 5C, b).

4 | DISCUSSION

Among mammalian classical *DNMs*, *DNM1* is the neuron-specific isoform with a pivotal role in synapsis formation and function (Ferguson et al., 2007). Recent studies suggest that mutations in *DNM1* gene in mice and humans are associated with neurodevelopmental disorders, as described for other genes involved in synaptic vesicle recycling (AlTassan et al., 2022; Von Spiczak et al., 2017; Yigit et al., 2022).

In zebrafish, two co-orthologs of human *DNM1* have been identified, named *dnm1a* and *dnm1b*. *Dnm1a* results more conserved to mammalian orthologs in terms of synteny and nucleotide sequence than *dnm1b*. Moreover, different transcripts were identified in *dnm1a*, resulting from alternative splicing. In particular, the splicing site that involves exons 10 and 11 has been described also in mice and human orthologs. Notably, mutations in these alternative spliced exons have been linked to the developmental and epileptic encephalopathy (DEE) disease in mammals, with more severe phenotype depending on the spliced exon carrying the mutations (Allen et al., 2016; Asinof et al., 2016; Boumil et al., 2010; Griffin et al., 2021; Kolnikova et al., 2018; Parthasarathy et al., 2022; Sahly et al., 2020).

Our WISH analyses showed a nervous tissue-specific expression only for *dnm1a*, characterized by a transcript distribution resembling genes involved in synaptic transmission, such as *ache* and *synj1* (Behra et al., 2002; Choudhry et al., 2021). Combining these data with the protein localization, it is reasonable to hypothesize that Dnm1a could be involved in the formation of both axon and synapse. In fact, starting from the 20-somite stage, the distribution of *dnm1a* transcript coincides with the first neuronal clusters in the developing brain and spinal cord, while the protein is also detectable in axon tracts and commissures of the cephalic nervous system and in the axons of spinal motor neurons.

Since the expression of *dnm1b* has been detected only by RT-PCR, and no evident signals in the nervous system emerged from WISH analyses, we hypothesize that low level of *dnm1b* transcript is present during embryonic development. Thus, data emerging from in silico and expression analyses, lead us to characterize the function of *dnm1a* during the nervous system development. Knockdown assays were performed by means of two morpholinos targeting specific regions exclusively in *dnm1a* transcript. From 24 hpf, *dnm1a*-MOs displayed severe motility defects, strongly suggesting a link with those observed in *Drosophila* and *C. elegans* dynamin mutants in which the block of endocytosis at presynaptic terminal results in a paralytic phenotype. The similarity between behavioral defects of *dnm1a* morphants and several zebrafish mutants for the formation of neuromuscular synapses (Panzer et al., 2005), suggests the involvement of *dnm1a* in this process. In addition, this is consistent with *dnm1a* expression in the area where the spinal motor neuron nuclei develop. To analyze the formation of neuromuscular junction (NMJ) after the *dnm1a* knockdown we firstly immunostained motor neuron axons. Although the axons were properly formed and exit from the spinal cord, we observed defects in their targeting, suggesting that *dnm1a* could have a role in both neurite outgrowth and pathfinding. A work by Torre and colleagues strongly supports this hypothesis, demonstrating that the treatment of cultured hippocampal neurons with two different antisense oligonucleotides against *dynamin* transcript resulted in a significant reduction in the number and length of neurites (Torre et al., 1994). In addition, it was shown that neurons carrying temperature-sensitive mutation in the

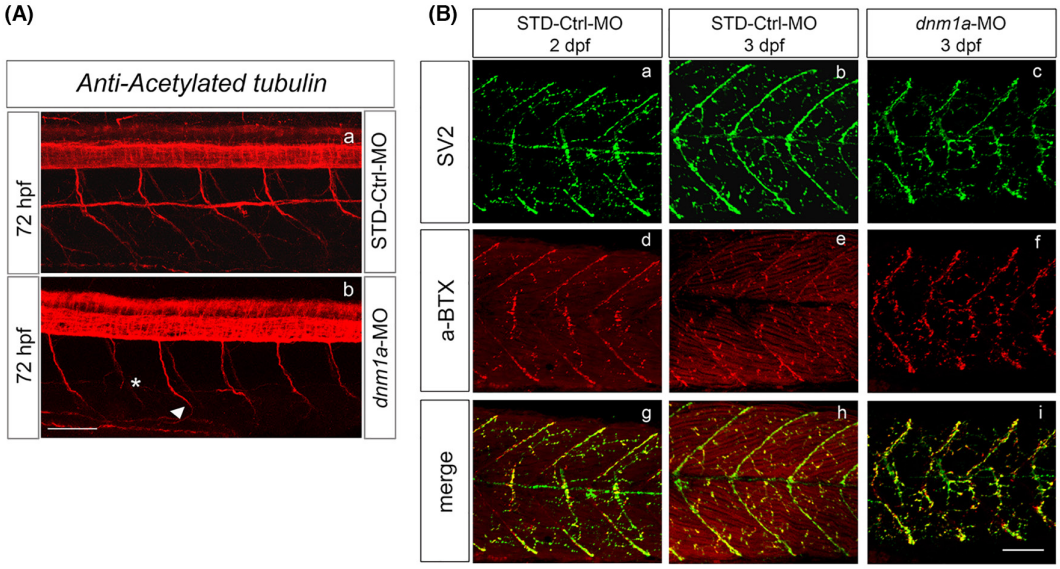

FIGURE 4 Panel A. Neurite formation in *dnm1a*-MO-injected embryos. (A) The neurite formation on 3 dpf morphants pertaining to the C1 class was observed after acetylated tubulin staining. (a and b) Morphants at 3 dpf were compared to control embryos. In *dnm1a*-Mos-injected embryos, different defects in the pathfinding of motor neuron axons were observed. The morphants showed a straight ventral trajectory of CaP axons (78% of injected embryos, $n=42$) compared to control embryos ($n=40$). Fewer morphants (14.3% of injected embryos, $n=42$) showed axons that stopped to elongate (asterisk), and an atypical curve of the terminal portion (arrowhead). Scale bar 100 μm. Panel B. *Presynaptic vesicles (SV2) and AChRs (α-BTX) in dnm1a-MO-injected embryos.* (a–i) In order to visualize NMJs under a confocal microscope, morphants and control embryos were double-stained with SV2 and α-bungarotoxin. (i) The merged signal observed in morphants suggested that the axonal projections were associated correctly with the cluster of AChR. (d–f) The number of NMJs did not appear to be different in the two experimental groups. The distribution pattern of AChR and NMJs appeared slightly altered in morphants compared with controls. This was explained as a secondary effect of the strong muscular defects. Scale bar 100 μm.

TABLE 3 Axon defects observed in embryos during development.

	Trajectory defect	Normal trajectory
STD-Ctrl-MO	1	41
dnm1a-MO	33***a***	9
	Grade defects	**Normal grade**
STD-Ctrl-MO	1	41
dnm1a-MO	33***a***	9
	Reduced extension	**Normal extension**
STD-Ctrl-MO	0	42
dnm1a-MO	6***b***	36
	Branch defects	**Normal branch**
STD-Ctrl-MO	0	42
dnm1a-MO	3	39

Note: Table reporting defect observed in axon development (defects in trajectory, grade, extension, and branching) on 42 embryos at 72 hpf, pertaining to three different experiments. ***a***, ***b*** denotes statistically significant differences. In particular, regarding both "Trajectory defect" and "Grade defects," STD-Ctrl-MO vs *dnm1a*-MO (*a*, $p<.001$, Chi-square value = 45.29, $df=1$); while regarding "Reduced extension," STD-Ctrl-MO versus *dnm1a*-MO (***b***, $p=.011$, Chi-square value = 6.46, $df=1$).

Drosophila dynamin gene, *shibire*, failed to outgrow neurites when cultured at the restrictive temperature (Masur et al., 1990). How DNM and endocytosis could contribute to neurite formation is still under investigation, but several hypotheses have been made. One possibility is that DNM may be involved in the endocytic recycling of proteins that are necessary for neurite formation, as growth factor receptors and other plasma membrane proteins. A second hypothesis suggests that DNM can take part in the neuronal growth factor-mediated signal transduction pathway. The last hypothesis is that DNM may play a role in assembling the microtubule backbone of the neurite (Hegarty et al., 2017; Torre et al., 1994). This is consistent with our observation of *dnm1a* along motor neuron axons. Although La and colleagues described for the first time the Dnm1 association with microtubules in vitro (La et al., 2020), our results represent the first evidence of this interaction in vivo.

After the neuritogenesis of spinal motor neurons, we performed the immunolocalization of NMJs. These structures, as well as AchRs, displayed an irregular distribution in *dnm1a*-MOs in comparison to control embryos. However, it cannot be excluded that this phenotype is secondary to the defects observed in spinal motor neuron axons or muscles. Histological and cytological analysis showed that myofibril organization in developing skeletal muscles was strongly affected in *dnm1a*-MOs. This phenotype suggested a new and intriguing role of *dnm1a* in muscle development. Given that the expression pattern of an early somitic marker as *myoD* did not display substantial differences in morphants and control embryos at 8 somites and 24 hpf stages, we hypothesized that the somite cells developed muscular features after *dnm1a* loss of function, but failed to assemble the contractile structures in myofibrils. Surprisingly,

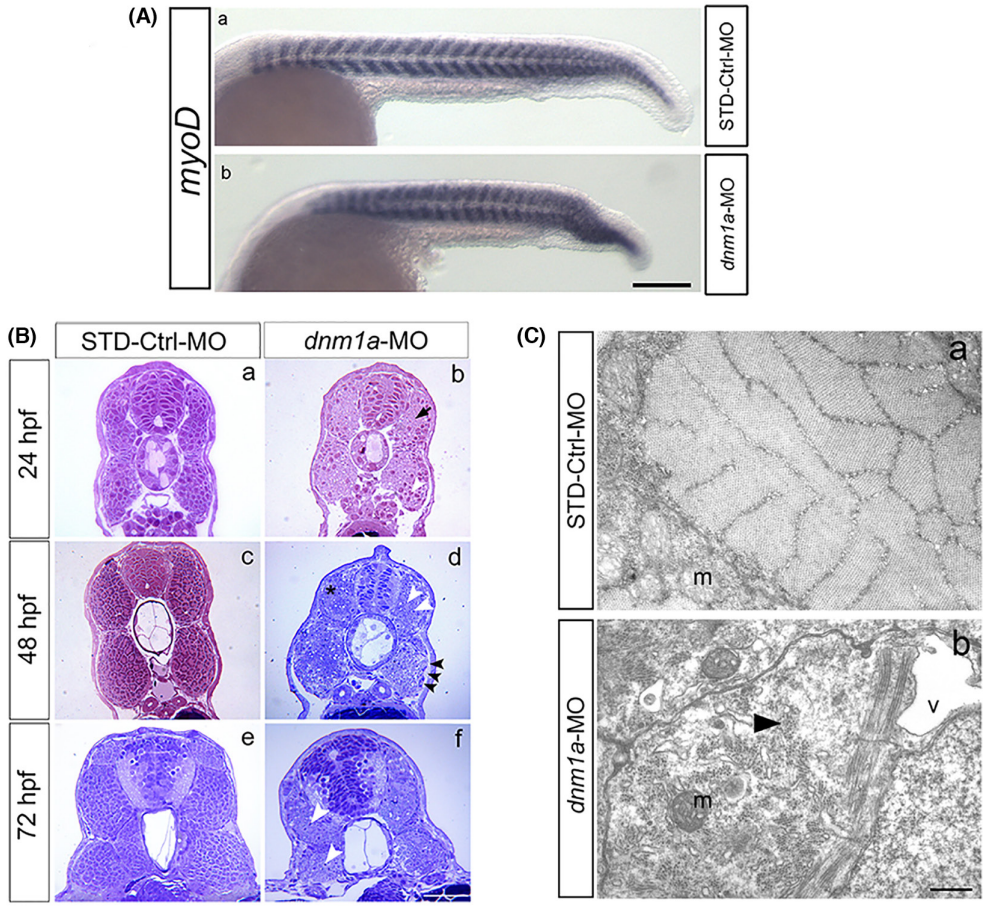

FIGURE 5 Morphants axial musculature development. The *myoD* expression pattern was analyzed after the *dnm1a*-MO microinjection. (A) At the developmental stage of 24 hpf, the distribution of *myoD* transcript was comparable between the *dnm1a*-MO-injected embryos and STD-Ctrl embryos. Scale bar 200 μm. (B, b, black arrow) In the myotome structure of *dnm1a*-MO embryos, compared to STD-Ctrl embryos, some atrophic fibers and broad spaces between muscle cells were observed. Moreover, the amount of myofibers in the muscle pioneers was drastically reduced. (B, c, f and e) At 2 dpf morphants showed alteration in the myotome structure, compared to STD-Ctrl embryos. (asterisk) In *dnm1a*-MO-injected embryos, darker cells were observed on the upper portion of the myotome, corresponding to the adaxial cells after migration. (black arrowhead) Slow fibers development appeared strongly impaired in the deepest region of the myotome. (white arrowhead) Large amounts of not differentiated myoblasts with a central nucleus were present, alongside an evident nucleolus and a few groups of disorganized myofibrils. Furthermore, in morphants were detected increased intercellular spaces, compared to STD-Ctrl embryos. (B, a–f) Histological analyses were performed on morphants and control embryos at 2, and 3 dpf. In morphants were observed a strongly altered organization of muscle fibers, with an increase in intercellular spaces and the impairment of myofiber orientation. (B, d) The deep portion of 2 dpf STD-Ctrl embryos myotome displayed muscle cells with a central nucleus and myofibers forming regular ring-like structures. Fast muscle fibers are positioned in the deep portion of the myotome, whereas slow muscle fibers are smaller and darker, forming a superficial monolayer on the surface of the myotome. Scale bar 100 μm. (C, b) At ultrastructural level, 72 hpf morphants showed mitochondria and nuclei in the central region of the muscle cells and regions in which were present myofibrils with a correct orientation, interrupted by extensive regions of vacuolated sarcoplasm (v). (C, a) Contrarily, in STD-Ctrl embryos, long myofibrils were correctly positioned, occupying the intracellular space of the myofibers. (C, a and b) Fast muscle fibers were observed in the deep portion of the myotome and slow muscle fibers on the surface of the myotome. Mitochondria were positioned in the subcortical region of the muscle cells, whereas sarcoplasmic reticulum enveloped myofibrils (m). Scale bar 1 μm.

similar muscular phenotypes have been already described in mutants with a disrupted activity of neuromuscular junction, supporting the importance of nerve function for refining myofibril organization of the different embryonic muscle types (Behra et al., 2002; Brennan et al., 2005). For instance, myofibers are significantly disrupted in mutants of *ache* gene, in which acetylcholine (ACh) hydrolysis in the synaptic cleft is completely abolished. In addition, the *nic1* mutant, that lacks the α-subunit of the acetylcholine receptor (AChR), displayed evident defects in late myofibrillogenesis (Choudhry et al., 2021). Interestingly, these defects have been correlated with changes in the cytoplasmic Ca^{2+} levels of muscle cells. The action potential that originates in the sarcolemma after the binding between ACh and AChRs, penetrates deeper into the muscle through the T-tubule system, and causes Ca^{2+} release from the sarcoplasmic reticulum. Brennan and colleagues proposed that *desmin* intermediate

filaments, making up the exosarcomeric cytoskeleton are responsible for the alignment of myofibrils (Brennan et al., 2005). Interestingly *desmin* activity seems to be regulated by calcium-binding protein (Li et al., 1997; Zhang et al., 2021).

According to the expression pattern and the functional analyses, we hypothesize that Dnm1a is essential for the proper functioning of the neuromuscular synapse. In particular, Dnm1a might be transported along motorneuron axons toward the presynaptic terminal of NMJs, where it could be involved in the recycling of synaptic vesicles by endocytosis. This is a crucial step to avoid vesicle depletion and consequently paralysis of neurotransmission.

Moreover, we hypothesize that muscular defect of *dnm1a*-MOs could be dependent on the block of nerve activity that is fundamental to control the Ca^{2+} releasing in the cytoplasm of muscular cells and thus the organization of contractile structures.

To conclude, the importance behind the characterization of zebrafish *dnm1a* gene reported in this paper relies in the fact that zebrafish can be an impressive model not only to deeply understand the involvement of *dnm1a* in neurodevelopment, but also for the study of pathologic mechanisms related to *DNM1* defects. Interestingly, severe neurodevelopmental phenotypes, comprising early-onset epilepsy, muscular hypotonia, visual impairment, and marked developmental delay, have been described in three patients with DNM1 loss of function mutations (AlTassan et al., 2022; Yigit et al., 2022). Future studies may clarify whether the neurodevelopment defects observed after the *dnm1a* knockdown precisely recapitulate those in patients, possibly promoting the identification of new therapeutic targets.

About the developmental epileptic encephalopathy (DEE) research, the presence of the alternative splicing in 10–11 exon, together with the nervous specific expression, makes *dnm1a* a valid target for future studies aimed at identifying new genetic models of DEE. In this regard, zebrafish could represent a reliable experimental model for studying genotype–phenotype correlations in this neurodevelopmental disease.

DECLARATION OF TRANSPARENCY

The authors, reviewers and editors affirm that in accordance to the policies set by the *Journal of Neuroscience Research*, this manuscript presents an accurate and transparent account of the study being reported and that all critical details describing the methods and results are present.

AUTHOR CONTRIBUTIONS

All authors had full access to all the data in the study and take responsibility for the integrity of the data and accuracy of the data. *Conceptualization*, C.B., G.G. and A.P.; *Methodology*, G.G., C.B.; *Investigation*, G.G., C.B., S. Carra and J.B.; *Formal Analysis*, C.B., G.G., S.C. and G.B.; *Resources*: G.G., S.C. and F.C.; *Writing – Original Draft*, C.B. and G.G.; *Writing – Review & Editing*, C.B., G.G., S.C., A.P., G.B., F.C.; *Visualization*, G.V., P.M.; *Supervision*, G.G.; *Funding Acquisition*, F.C.

ACKNOWLEDGMENTS

We thank Prof. Pier Paolo Di Fiore (IEO Institute, Milan, Italy), for his precious support and advisement, and Dr. Maurizio Gualtieri for the statistical support during the revision phase of the manuscript. Open Access Funding provided by Universita degli Studi di Milano-Bicocca within the CRUI-CARE Agreement.

CONFLICT OF INTEREST STATEMENT

The authors have no conflict of interest to declare.

PEER REVIEW

The peer review history for this article is available at https://www.webofscience.com/api/gateway/wos/peer-review/10.1002/jnr.25197.

DATA AVAILABILITY STATEMENT

The data that support the findings of this study are available from the corresponding author upon reasonable request.

REFERENCES

Allen, N. M., Conroy, J., Shahwan, A., Lynch, B., Correa, R. G., Pena, S. D., McCreary, D., Magalhaes, T. R., Ennis, S., Lynch, S. A., & King, M. D. (2016). Unexplained early onset epileptic encephalopathy: Exome screening and phenotype expansion. *Epilepsia*, *57*, e12–e17. https://doi.org/10.1111/epi.13250

AlTassan, R., AlQudairy, H., Alromayan, R., Alfalah, A., AlHarbi, O. A., González-Álvarez, A. C., Arold, S. T., & Kaya, N. (2022). Clinical, radiological, and genetic characterization of a patient with a novel homoallelic loss-of-function variant in DNM1. *Genes*, *13*(12), 2252. https://doi.org/10.3390/genes13122252

Asinof, S., Mahaffey, C., Beyer, B., Frankel, W. N., & Boumil, R. (2016, November). Dynamin 1 isoform roles in a mouse model of severe childhood epileptic encephalopathy. *Neurobiology of Disease*, *95*, 1–11. https://doi.org/10.1016/j.nbd.2016.06.014

Balciuniene, J., Nagelberg, D., Walsh, K. T., Camerota, D., Georlette, D., Biemar, F., Bellipanni, G., & Balciunas, D. (2013, September 14). Efficient disruption of zebrafish genes using a Gal4-containing gene trap. *BMC Genomics*, *14*, 619. https://doi.org/10.1186/1471-2164-14-619

Behra, M., Cousin, X., Bertrand, C., Vonesch, J. L., Biellmann, D., Chatonnet, A., & Strähle, U. (2002, February). Acetylcholinesterase is required for neuronal and muscular development in the zebrafish embryo. *Nature Neuroscience*, *5*(2), 111–118. https://doi.org/10.1038/nn788

Boumil, R. M., Letts, V. A., Roberts, M. C., Lenz, C., Mahaffey, C. L., Zhang, Z. W., Moser, T., & Frankel, W. N. (2010, August 5). A missense mutation in a highly conserved alternate exon of dynamin-1 causes epilepsy in fitful mice. *PLoS Genetics*, *6*(8), e1001046. https://doi.org/10.1371/journal.pgen.1001046

Bragato, C., Blasevich, F., Ingenito, G., Mantegazza, R., & Maggi, L. (2021, May). Therapeutic efficacy of 3,4-Diaminopyridine phosphate on neuromuscular junction in Pompe disease. *Biomedicine & Pharmacotherapy*, *137*, 111357. https://doi.org/10.1016/j.biopha.2021.111357

Bragato, C., Gaudenzi, G., Blasevich, F., Pavesi, G., Maggi, L., Giunta, M., Cotelli, F., & Mora, M. (2016, February 4). Zebrafish as a model to investigate dynamin 2-related diseases. *Scientific Reports*, *6*, 20466. https://doi.org/10.1038/srep20466

Brennan, C., Mangoli, M., Dyer, C. E., & Ashworth, R. (2005, November 15). Acetylcholine and calcium signalling regulates muscle fibre

formation in the zebrafish embryo. *Journal of Cell Science*, *118*(Pt 22), 5181–5190. https://doi.org/10.1242/jcs.02625

Chen, M. S., Burgess, C. C., Vallee, R. B., & Wadsworth, S. C. (1992, November). Developmental stage- and tissue-specific expression of shibire, a Drosophila gene involved in endocytosis. *Journal of Cell Science*, *103*(Pt 3), 619–628. https://doi.org/10.1242/jcs.103.3.619

Chen, M. S., Obar, R. A., Schroeder, C. C., Austin, T. W., Poodry, C. A., Wadsworth, S. C., & Vallee, R. B. (1991, June 13). Multiple forms of dynamin are encoded by shibire, a Drosophila gene involved in endocytosis. *Nature*, *351*(6327), 583–586. https://doi.org/10.1038/351583a0

Choudhry, H., Aggarwal, M., & Pan, P. Y. (2021, November 20). Mini-review: Synaptojanin 1 and its implications in membrane trafficking. *Neuroscience Letters*, *765*, 136288. https://doi.org/10.1016/j.neulet.2021.136288

Clark, S. G., Shurland, D. L., Meyerowitz, E. M., Bargmann, C. I., & van der Bliek, A. M. (1997, September 16). A dynamin GTPase mutation causes a rapid and reversible temperature-inducible locomotion defect in *C. elegans*. *Proceedings of the National Academy of Sciences of the United States of America*, *94*(19), 10438–10443. https://doi.org/10.1073/pnas.94.19.10438

Cousin, M. A. (2017, August 3). Integration of synaptic vesicle cargo retrieval with endocytosis at central nerve terminals. *Frontiers in Cellular Neuroscience*, *11*, 234. https://doi.org/10.3389/fncel.2017.00234

Damke, H., Baba, T., Warnock, D. E., & Schmid, S. L. (1994, November). Induction of mutant dynamin specifically blocks endocytic coated vesicle formation. *The Journal of Cell Biology*, *127*(4), 915–934. https://doi.org/10.1083/jcb.127.4.915

Ferguson, S. M., Brasnjo, G., Hayashi, M., Wölfel, M., Collesi, C., Giovedi, S., Raimondi, A., Gong, L. W., Ariel, P., Paradise, S., O'Toole, E., Flavell, R., Cremona, O., Miesenböck, G., Ryan, T. A., & De Camilli, P. (2007). A selective activity-dependent requirement for dynamin 1 in synaptic vesicle endocytosis. *Science*, *316*, 570–574. https://doi.org/10.1126/science.1140621

Ferguson, S. M., & De Camilli, P. (2012, January 11). Dynamin, a membrane-remodelling GTPase. *Nature Reviews. Molecular Cell Biology*, *13*(2), 75–88. https://doi.org/10.1038/nrm3266

Gibbs, E. M., Davidson, A. E., Trickey-Glassman, A., Backus, C., Hong, Y., Sakowski, S. A., Dowling, J. J., & Feldman, E. L. (2013). Two dynamin-2 genes are required for normal zebrafish development. *PLoS One*, *8*(2), e55888. https://doi.org/10.1371/journal.pone.0055888

Griffin, A., Carpenter, C., Liu, J., Paterno, R., Grone, B., Hamling, K., Moog, M., Dinday, M. T., Figueroa, F., Anvar, M., Ononuju, C., Qu, T., & Baraban, S. C. (2021, June 3). Phenotypic analysis of catastrophic childhood epilepsy genes. *Communications Biology*, *4*(1), 680. https://doi.org/10.1038/s42003-021-02221-y

Hegarty, S. V., Sullivan, A. M., & O'Keeffe, G. W. (2017, March 16). Endocytosis contributes to BMP2-induced Smad signalling and neuronal growth. *Neuroscience Letters*, *643*, 32–37. https://doi.org/10.1016/j.neulet.2017.02.013

Hinshaw, J. E., & Schmid, S. L. (1995, March 9). Dynamin self-assembles into rings suggesting a mechanism for coated vesicle budding. *Nature*, *374*(6518), 190–192. https://doi.org/10.1038/374190a0

Howe, K., Clark, M. D., Torroja, C. F., Torrance, J., Berthelot, C., Muffato, M., Collins, J. E., Humphray, S., McLaren, K., Matthews, L., McLaren, S., Sealy, I., Caccamo, M., Churcher, C., Scott, C., Barrett, J. C., Koch, R., Rauch, G. J., White, S., … Stemple, D. L. (2013, April 25). The zebrafish reference genome sequence and its relationship to the human genome. *Nature*, *496*(7446), 498–503. https://doi.org/10.1038/nature12111. Erratum in: Nature. 2014 January 9;505(7482):248.

Kaksonen, M., & Roux, A. (2018, May). Mechanisms of clathrin-mediated endocytosis. *Nature Reviews. Molecular Cell Biology*, *19*(5), 313–326. https://doi.org/10.1038/nrm.2017.132

Kimmel, C. B., Ballard, W. W., Kimmel, S. R., Ullmann, B., & Schilling, T. F. (1995, July). Stages of embryonic development of the zebrafish. *Developmental Dynamics*, *203*(3), 253–310. https://doi.org/10.1002/aja.1002030302

Koenig, J. H., & Ikeda, K. (1989, November). Disappearance and reformation of synaptic vesicle membrane upon transmitter release observed under reversible blockage of membrane retrieval. *The Journal of Neuroscience*, *9*(11), 3844–3860. https://doi.org/10.1523/JNEUROSCI.09-11-03844.1989

Kolnikova, M., Skopkova, M., Ilencikova, D., Foltan, T., Payerova, J., Danis, D., Klimes, I., Stanik, J., & Gasperikova, D. (2018, March). DNM1 encephalopathy—Atypical phenotype with hypomyelination due to a novel de novo variant in the DNM1 gene. *Seizure*, *56*, 31–33. https://doi.org/10.1016/j.seizure.2018.01.020

Koonin, E. V. (2005). Orthologs, paralogs, and evolutionary genomics. *Annual Review of Genetics*, *39*, 309–338. https://doi.org/10.1146/annurev.genet.39.073003.114725

Köster, R. W., & Fraser, S. E. (2001, November 27). Direct imaging of in vivo neuronal migration in the developing cerebellum. *Current Biology*, *11*(23), 1858–1863. https://doi.org/10.1016/s0960-9822(01)00585-1

La, T. M., Tachibana, H., Li, S. A., Abe, T., Seiriki, S., Nagaoka, H., Takashima, E., Takeda, T., Ogawa, D., Makino, S. I., Asanuma, K., Watanabe, M., Tian, X., Ishibe, S., Sakane, A., Sasaki, T., Wada, J., Takei, K., & Yamada, H. (2020). Dynamin 1 is important for microtubule organization and stabilization in glomerular podocytes. *The FASEB Journal*, *34*, 16449–16463.

Li, Z., Mericskay, M., Agbulut, O., Butler-Browne, G., Carlsson, L., Thornell, L. E., Babinet, C., & Paulin, D. (1997, October 6). Desmin is essential for the tensile strength and integrity of myofibrils but not for myogenic commitment, differentiation, and fusion of skeletal muscle. *The Journal of Cell Biology*, *139*(1), 129–144. https://doi.org/10.1083/jcb.139.1.129

Masur, S. K., Kim, Y. T., & Wu, C. F. (1990, April). Reversible inhibition of endocytosis in cultured neurons from the Drosophila temperature-sensitive mutant shibirets1. *Journal of Neurogenetics*, *6*(3), 191–206. https://doi.org/10.3109/01677069009107110

Narayanan, R., & Oates, A. C. (2019, March 20). Detection of mRNA by whole mount in situ hybridization and DNA extraction for genotyping of zebrafish embryos. *Bio-Protocol*, *9*(6), e3193. https://doi.org/10.21769/BioProtoc.3193

Panzer, J. A., Gibbs, S. M., Dosch, R., Wagner, D., Mullins, M. C., Granato, M., & Balice-Gordon, R. J. (2005, September 15). Neuromuscular synaptogenesis in wild-type and mutant zebrafish. *Developmental Biology*, *285*(2), 340–357. https://doi.org/10.1016/j.ydbio.2005.06.027

Parthasarathy, S., Ruggiero, S. M., Gelot, A., Soardi, F. C., Ribeiro, B. F. R., Pires, D. E. V., Ascher, D. B., Schmitt, A. S., Rambaud, C., Xie, H. M., Lusk, L., Wilmarth, O., McDonnell, P. P., Juarez, O. A., Grace, A. N., Buratti, J., Mignot, C., Gras, D., Nava, C., … Cuddapah, V. A. (2022). A recurrent de novo splice site variant involving DNM1 exon 10a causes developmental and epileptic encephalopathy through a dominant-negative mechanism. *BioRxiv preprints*. https://doi.org/10.1101/2022.06.02.492389

Ramachandran, R., & Schmid, S. L. (2018, April 23). The dynamin superfamily. *Current Biology*, *28*(8), R411–R416. https://doi.org/10.1016/j.cub.2017.12.013

Robu, M. E., Larson, J. D., Nasevicius, A., Beiraghi, S., Brenner, C., Farber, S. A., & Ekker, S. C. (2007, May 25). p53 activation by knockdown technologies. *PLoS Genetics*, *3*(5), e78. https://doi.org/10.1371/journal.pgen.0030078

Sahly, A. N., Krochmalnek, E., St-Onge, J., Srour, M., & Myers, K. A. (2020, December). Severe DNM1 encephalopathy with dysmyelination

due to recurrent splice site pathogenic variant. *Human Genetics*, *139*(12), 1575–1578. https://doi.org/10.1007/s00439-020-02224-5

Schindelin, J., Arganda-Carreras, I., Frise, E., Kaynig, V., Longair, M., Pietzsch, T., Preibisch, S., Rueden, C., Saalfeld, S., Schmid, B., Tinevez, J. Y., White, D. J., Hartenstein, V., Eliceiri, K., Tomancak, P., & Cardona, A. (2012, June 28). Fiji: An open-source platform for biological-image analysis. *Nature Methods*, *9*(7), 676–682. https://doi.org/10.1038/nmeth.2019

Shehwana, H., & Konu, O. (2019). Comparative transcriptomics between zebrafish and mammals: A roadmap for discovery of conserved and unique signaling pathways in physiology and disease. *Frontiers in Cell and Developmental Biology*, *7*, 5. https://doi.org/10.3389/fcell.2019.00005

Suster, M. L., Kikuta, H., Urasaki, A., Asakawa, K., & Kawakami, K. (2009). Transgenesis in zebrafish with the tol2 transposon system. *Methods in Molecular Biology*, *561*, 41–63. https://doi.org/10.1007/978-1-60327-019-9_3

Thisse, B., & Thisse, C. (2014). In situ hybridization on whole-mount zebrafish embryos and young larvae. *Methods in Molecular Biology*, *1211*, 53–67. https://doi.org/10.1007/978-1-4939-1459-3_5

Torre, E., McNiven, M. A., & Urrutia, R. (1994, December 23). Dynamin 1 antisense oligonucleotide treatment prevents neurite formation in cultured hippocampal neurons. *The Journal of Biological Chemistry*, *269*(51), 32411–32417.

van der Bliek, A. M., & Meyerowitz, E. M. (1991, May 30). Dynamin-like protein encoded by the Drosophila shibire gene associated with vesicular traffic. *Nature*, *351*(6325), 411–414. https://doi.org/10.1038/351411a0

Von Spiczak, S., Helbig, K. L., Shinde, D. N., Huether, R., Pendziwiat, M., Lourenço, C., Nunes, M. E., Sarco, D. P., Kaplan, R. A., Dlugos, D. J., Kirsch, H., Slavotinek, A., Cilio, M. R., Cervenka, M. C., Cohen, J. S., McClellan, R., Fatemi, A., Yuen, A., Sagawa, Y., … Epi4K Consortium; EuroEPINOMICS-RES NLES Working Group. (2017, July 25). DNM1 encephalopathy: A new disease of vesicle fission. *Neurology*, *89*(4), 385–394. https://doi.org/10.1212/WNL.0000000000004152

Westerfield, M., Stuart, G., & Wegner, J. (1993). Expression of foreign genes in zebrafish embryos. In W. C. Brown (Ed.), *Developments in industrial microbiology* (Vol. *II*, pp. 658–665). Springer.

Woods, I. G., Lyons, D. A., Voas, M. G., Pogoda, H. M., & Talbot, W. S. (2006, April 4). nsf is essential for organization of myelinated axons in zebrafish. *Current Biology*, *16*(7), 636–648. https://doi.org/10.1016/j.cub.2006.02.067

Yigit, G., Sheffer, R., Daana, M., Li, Y., Kaygusuz, E., Mor-Shakad, H., Altmüller, J., Nürnberg, P., Douiev, L., Kaulfuss, S., Burfeind, P., Wollnik, B., & Brockmann, K. (2022, June). Loss-of-function variants in DNM1 cause a specific form of developmental and epileptic encephalopathy only in biallelic state. *Journal of Medical Genetics*, *59*(6), 549–553. https://doi.org/10.1136/jmedgenet-2021-107769

Zhang, H., Bryson, V. G., Wang, C., Li, T., Kerr, J. P., Wilson, R., Muoio, D. M., Bloch, R. J., Ward, C., & Rosenberg, P. B. (2021, September 8). Desmin interacts with STIM1 and coordinates Ca2+ signaling in skeletal muscle. *JCI Insight*, *6*(17), e143472. https://doi.org/10.1172/jci.insight.143472

Zhang, R., Lee, D. M., Jimah, J. R., Gerassimov, N., Yang, C., Kim, S., Luvsanjav, D., Winkelman, J., Mettlen, M., Abrams, M. E., Kalia, R., Keene, P., Pandey, P., Ravaux, B., Kim, J. H., Ditlev, J. A., Zhang, G., Rosen, M. K., Frost, A., … Chen, E. H. (2020, June). Dynamin regulates the dynamics and mechanical strength of the actin cytoskeleton as a multifilament actin-bundling protein. *Nature Cell Biology*, *22*(6), 674–688. https://doi.org/10.1038/s41556-020-0519-7

SUPPORTING INFORMATION

Additional supporting information can be found online in the Supporting Information section at the end of this article.

FIGURE S1. Evolutionary relationships of taxa. (A) Protein sequence databases were downloaded from NCBI or ENSEMBL databases, from the organism specific databases (Borowiec et al., 2015), from Compagen (http://www.compagen.org/) or from the Joint Genome Institute (http://genome.jgi.doe.gov/) databases; Dynamin homologues were retrieved by blast analysis; accession numbers and sequences will be provided upon specific request. The evolutionary history was inferred using the Minimum Evolution method [S1] using MEGA7 [S2]. The bootstrap consensus tree inferred from 50 replicates [S3] is taken to represent the evolutionary history of the taxa analyzed [S3]. Branches corresponding to partitions reproduced in less than 50% bootstrap replicates are collapsed. The evolutionary distances were computed using the Poisson correction method [S4] and are in the units of the number of amino acid substitutions per site. The ME tree was searched using the Close-Neighbor-Interchange (CNI) algorithm [S5] at a search level of 1. The Neighbor-joining algorithm [S6] was used to generate the initial tree. The analysis involved 48 amino acid sequences. All positions with less than 95% site coverage were eliminated. That is, fewer than 5% alignment gaps, missing data, and ambiguous bases were allowed at any position. There were a total of 477 positions in the final dataset. (B) Synteny map obtained by the Genomicus Phyloview browser that compares flanking regions of *dnm1a* and *dnm1b* loci among teleostei. Paralogs genes are annotated without surrounding lines, while orthologs are annotated with a black surrounding line. The syntenic map is supporting the hypothesis that the origin of *dnm1a* and *dnm1b* occurred from the teleost lineage whole-genome duplication 320 million years ago.

FIGURE S2. *dnm1b* spatio-temporal expression. RT-PCR assays using total RNAs extracted from embryos at different embryonic and larval stages (ranging from 64–128 cells stages to early larval period) were performed. During embryo development, *dnm1b* mRNA was identified starting from the 80% of epiboly stage (circa 9 hpf) through 5 dpf.

Transparent Science Questionnaire for Authors

How to cite this article: Bragato, C., Pistocchi, A., Bellipanni, G., Confalonieri, S., Balciuniene, J., Monastra, F. M., Carra, S., Vitale, G., Mantecca, P., Cotelli, F., & Gaudenzi, G. (2023). Zebrafish *dnm1a* gene plays a role in the formation of axons and synapses in the nervous tissue. *Journal of Neuroscience Research*, *101*, 1345–1359. https://doi.org/10.1002/jnr.25197